July 10, 1967

To the Graduate Council:

I am submitting herewith a thesis written by Kenneth E. Koch entitled "An Experimental Study of Flow Geometry and Transition in the Near Wake of a Sharp Slender Cone." I recommend that it be accepted for nine quarter hours of credit in partial fulfillment of the requirements for the degree of Master of Science, with a major in Aerospace Engineering.

J. Keith Potter
Major Professor

We have read this thesis and recommend its acceptance:

William J. Snyder

R. L. Young

Accepted for the Council:

Hilton A. Smith
Vice President for
Graduate Studies and Research

AN EXPERIMENTAL STUDY OF FLOW GEOMETRY AND TRANSITION IN THE NEAR WAKE OF A SHARP SLENDER CONE

A Thesis

Presented to

the Graduate Council of

The University of Tennessee

In Partial Fulfillment

of the Requirements for the Degree

Master of Science

---

by

Kenneth E. Koch

December 1967

1286594

ACKNOWLEDGMENT

The author wishes to express his appreciation to the officials of the Air Force and ARO, Inc., for the opportunity to attend The University of Tennessee Space Institute. The author is particularly indebted to: his advisor, J. L. Potter, Manager of the Aerophysics Branch and part-time faculty member of the Institute; A. B. Bailey, Fluid Dynamics Section Supervisor, for his many helpful discussions during the course of this study; and to O. H. Bock, Aerophysics Measurements Section, who designed and developed the schlieren systems used.

The research reported herein was sponsored by Headquarters AEDC, Arnold Air Force Station, Tennessee, under contract AF 40(600)-1200 with ARO, Inc. Further reproduction is authorized to satisfy needs of the U. S. Government.

TABLE OF CONTENTS

CHAPTER		PAGE
I.	INTRODUCTION	1
II.	ANALYSIS OF TRANSITION DATA	7
III.	NEAR WAKE GEOMETRY	26
IV.	DRAG ANALYSIS	36
V.	CONCLUSIONS	38
BIBLIOGRAPHY		40
APPENDIX		43
	DESCRIPTION OF TEST APPARATUS	44
	VKF 100-Foot Hypervelocity Range K	44
	VKF 1000-Foot Hypervelocity Range K	45

LIST OF FIGURES

FIGURE		PAGE
1.	Model A and Sabot	4
2.	Models B and C With Sabot	5
3.	Sketch of the Flow Field Showing Some of the Tabulated Parameters	9
4.	Parallel-light Shadowgram of Model A, $Re_{\infty,D} = 3.7 \times 10^6$, $M_\infty = 5.1$	11
5.	Point-light-source Shadowgram of Model A, $Re_{\infty,D} = 1.41 \times 10^6$, $M_\infty = 5.3$	12
6.	Horizontal Knife-edge Black-and-white Schlieren Photograph of Model A, $Re_{\infty,D} = 6.59 \times 10^5$, $M_\infty = 5.02$	13
7.	Vertical Knife-edge Black-and-white Schlieren Photograph of Model A, $Re_{\infty,D} = 7.05 \times 10^5$, $M_\infty = 5.28$	14
8.	Color Schlieren Photograph of Model A, $Re_{\infty,D} = 3.64 \times 10^5$, $M_\infty = 5.3$	15
9.	Black-and-white Schlieren Photograph of Model A, $Re_{\infty,D} = 1.7 \times 10^5$, $M_\infty = 5.6$	16
10.	Color Schlieren Photograph of Model A, $Re_{\infty,D} = 1.81 \times 10^5$, $M_\infty = 5.4$	17

FIGURE PAGE

11. Color Schlieren Photograph of Model A, $Re_{\infty,D} = 7.4 \times 10^4$, $M_\infty = 5.4$ 18

12. Two Frames of Black-and-white Drum Camera Schlieren Photograph of Model A, $Re_{\infty,D} = 3.71 \times 10^4$, $M_\infty = 5.7$ 19

13. Variation of Transition and Neck Reynolds Numbers With Freestream Body Reynolds Number 20

14. The Effect of Angle-of-attack on Transition Distance When Transition Occurs Near to the Base for Model A 22

15. The Variation of Neck Location as a Function of Freestream Body Reynolds Number 27

16. The Variation of Neck Diameter as a Function of Freestream Body Reynolds Number 28

17. The Variation of Wake Closure Angle as a Function of Freestream Body Reynolds Number . . 30

18. Map of the Base Flow Region 32

19. Sketch of the Flow Field Showing the Base Flow Pattern for High Reynolds Number 33

20. The Variation of Drag Coefficient With Freestream Length Reynolds Number 37

NOMENCLATURE

C_D	Drag coefficient
D	Body base diameter, inches
L	Body axial length, inches
L'	Trajectory length, feet
M	Mach number
r	Distance measured in radial direction, inches
Re	Reynolds number
T	Temperature, degrees Kelvin
U	Freestream velocity, feet/second
w	Wake neck diameter, inches
X	Axial distance measured from base, inches
X_{TR}	Distance to transition, measured from nose, inches
X_n	Distance to wake neck, measured from nose, inches
z	Distance along trajectory, feet
α	Angle of attack of model in individual photographs, degrees
δ	Local absolute angle of attack, degrees
$\overline{\delta^2}$	Mean squared angle of attack, $(\text{degrees})^2$
θ	Model half-angle, degrees
ρ	Mass density of range air, slugs/foot^3
Φ	Wake closure half-angle, degrees

Subscripts

aw	Adiabatic wall conditions
D	Using cone base diameter as reference length
o	Zero angle of attack
w	Model wall conditions
X_n	Using X_n as reference length
X_{TR}	Using X_{TR} as reference length
∞	Freestream conditions

CHAPTER I

INTRODUCTION

The survey papers concerned with hypersonic flow fields by Cheng (1)[1] and Lykoudis (2) state that among the areas requiring extensive experimental investigation is the base flow region for laminar, transitional, and fully turbulent flow conditions. Many mathematical approaches, discussed briefly in References (1) and (2), have been developed for analysis of the near wake (i.e., the flow region extending from the base downstream past the wake neck to the region where the local pressure has returned to the free-stream value). These investigations have shown that the primary source for high temperature fluid in the wake of a sharp slender body is the boundary layer. They indicate that the character of the far wake is controlled by the manner in which the boundary layer is processed through the base flow region, together with the location of transition from laminar to turbulent flow.

Wilson (3), using an aeroballistic range, has shown that for hypersonic blunt bodies the location of transition

---

[1]Numbers in parentheses refer to similarly numbered references in the bibliography.

will move upstream with increasing Reynolds number and eventually "stick" (i.e., occur at a position in the wake fixed with respect to the body) just downstream of the wake neck. As the Reynolds number is increased further, transition will finally jump forward onto the body. This phenomenon of "sticking" has not been fully investigated for sharp, slender bodies. Wilson (3) has reported that no evidence of sticking was seen for blunt bodies at $M_\infty \approx 20$ and $Re_{\infty,D} < 6.3 \times 10^5$. However, for these conditions the location of transition was never closer to the body than 30 diameters so that its behavior in the vicinity of the body base was not observed.

The present investigation was carried out to study the character of the base flow region as transition moved from the body to the near wake. All of the data were obtained in aeroballistic ranges. The primary instrumentation consisted of sensitive schlieren systems. The Appendix contains a brief description of the ranges used. The use of aeroballistic ranges together with the schlieren systems allowed observation of the flow field over a range of more than two orders of magnitude of Reynolds number at a fixed Mach number (and velocity) and fixed model size. The test gas was air with a nominal freestream temperature of 300° K. The study was conducted at a nominal freestream Mach number of 5.2. This kept flow field temperatures relatively low in order to minimize flow field chemistry effects on the

phenomenon under investigation. Also, at this Mach number, the bow shock did not lie so close to the body as to interfere with schlieren observations of the boundary layer and near wake flow.

Sketches of the models and sabots used in this investigation are shown in Figures 1 and 2. The surface finish on all models was 12 microinches RMS or better. All model noses were viewed and photographed on a comparator which provided a 100X enlargement to determine the exact shape of the nose. Prior to launching, each model was cleaned in an ultrasonic Freon Precision Cleaning Agent bath.

The first design of the 1.75-inch base diameter model was a scaled-up version of model B, but with a sealed base, and will be referred to as model B_1. The 0.30-inch base diameter multi-metal model will be referred to as model B_2. The initial shots using model B_1 showed that local shocks were occurring at the locations of the joints. It was suspected that an upsetting of the joints was occurring during the launch, even though there was no measurable surface discontinuity visible on the cones. The upsets were considered undesirable because of their possible tripping of the boundary layer. In the range of Reynolds number where these local shocks were seen ($Re_{\infty,D} > 2.0 \times 10^6$), natural transition was on the body. For $Re_{\infty,D} < 8.0 \times 10^5$, no shock waves were seen on the body and the boundary layer was completely

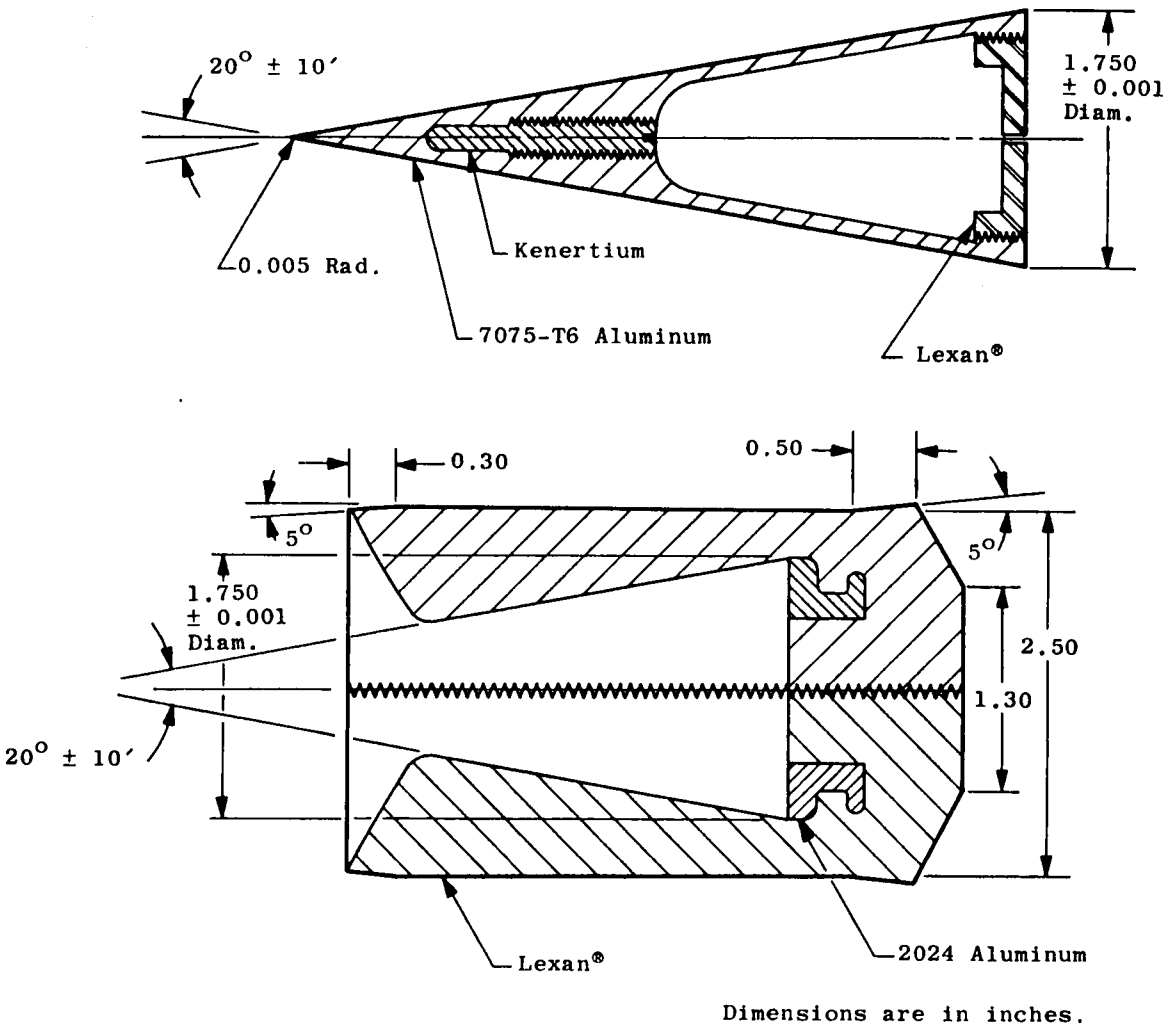
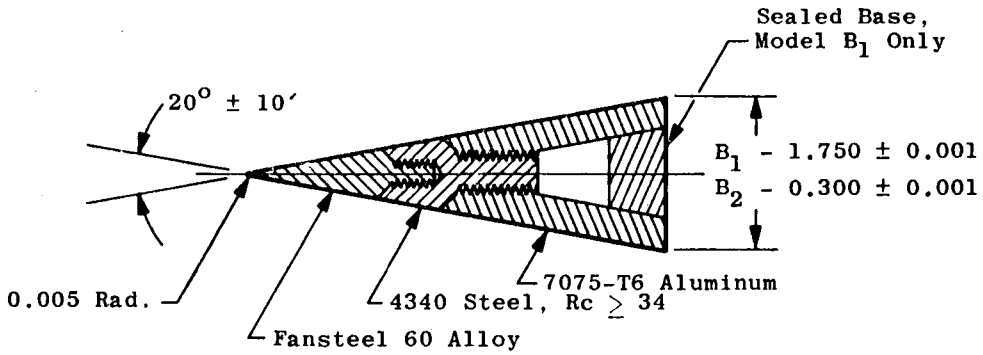
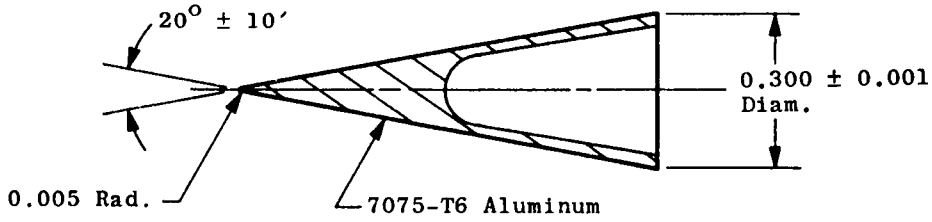


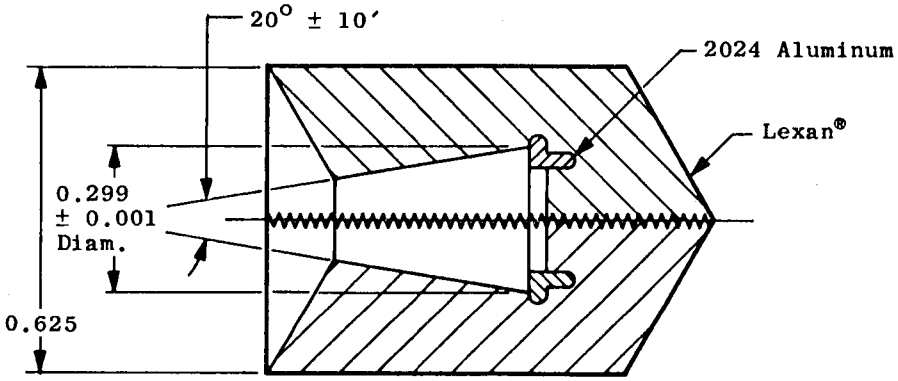
Figure 1. Model A and sabot.



a. Models B_1 and B_2.



b. Model C.



c. Sabot for models B and C.

Dimensions are in inches.

Figure 2. Models B and C with sabot.

laminar. Based on comparison with data from smooth models, shown later, the upsets had no effect on the location of transition or the geometry of the base flow field for these conditions.

In order to avoid the problem of the joints, the design was changed to the one shown in Figure 1, page 4, referred to as model A. The vent hole in the base was to provide a means of pressure relief so that the base bulkhead would not distort and to prevent any random leakage through the threads which would cause spurious results. Later in the program, prompted by concern over possible influence on the data, the time for venting the cavity was calculated and found to be much greater than the time of flight under some conditions. The venting mass flow rate under choked flow conditions was calculated to be 0.017 per cent of the mass flow rate swept out by the model, i.e., $\rho_\infty U_\infty \pi D^2/4$.

Fortunately, comparison of the data obtained from all of the models indicates that the vent hole in the base of model A had no effect on the flow field geometry or the location of transition.

CHAPTER II

ANALYSIS OF TRANSITION DATA

The models were launched at a nominal velocity of 5700 feet per second. The range pressure was varied between 730 and 5 millimeters of mercury. This corresponds to a freestream body base Reynolds number variation of 4.64×10^6 to 3.71×10^4 for the 1.75-inch base diameter cones. Table I lists the various parameters measured on each shot. Figure 3, page 9, is a sketch of the flow field showing the measurements tabulated in Table I. The mean squared angle of attack ($\overline{\delta^2}$) is defined by Equation 1,

$$\overline{\delta^2} = \frac{1}{L'} \int_0^{L'} \delta^2 \, dz \, . \qquad (1)$$

It is well known that boundary layer transition from laminar flow to full turbulence occurs over a length equal to many boundary layer thicknesses and a point of transition or transition location is an ambiguous term. Similarly, when transition occurs off the body, it requires many local characteristic thicknesses to proceed from fully laminar flow through the region of laminar instabilities to fully developed turbulent flow. (This can require hundreds of

TABLE I

TEST CONDITIONS AND MEASUREMENTS

Model	M_∞	$Re_{\infty, D} \times 10^{-5}$	$\overline{\delta_2}$ (deg.)^2	X_{TR}/D	X_n/D	w/D	Φ (deg.)	C_{D_o}
A	4.78	46.4	9.83	1.37	4.30	0.30	---	0.1300
A	5.06	37.0	1.93	1.45	4.80	0.30	---	0.1296
A	4.93	29.6	3.26	1.71	4.37	0.31	---	0.1363
A	5.11	24.0	8.07	1.94	4.84	0.29	---	----
A	5.20	17.5	0.30*	2.14	4.91	0.30	---	----
A	5.32	14.1	1.46	2.48	5.03	0.30	---	0.1145
A	5.33	14.2	11.71	2.04	4.83	0.31	---	0.1145
A	5.11	8.66	0.64	3.89	5.68	0.31	7.5	0.0950
A	5.30	3.64	6.20	5.23	5.91	0.39	6.75	----
A	5.43	1.81	3.89	6.15	6.68	0.42	6.0	----
A	4.96	10.0	3.81	3.86	5.29	0.31	8.75	----
A	4.97	11.3	4.13	3.74	5.13	0.31	10.0	0.0998
A	5.06	8.45	5.23	3.86	5.53	0.31	10.0	0.1060
A	5.39	0.74	3.41	7.65	8.23	0.54	3.25	----
A	5.26	11.8	5.45	2.87	5.33	0.36	10.0	0.1065
A	5.15	6.85	6.44	4.33	5.43	0.36	8.0	----
A	5.00	10.0	3.07	3.73	5.59	0.28	9.5	0.0980
A	5.11	23.6	0.59	1.49	4.88	0.29	---	0.1276
A	5.00	11.2	6.50*	2.66	5.30	0.32	10.0	----
A	5.70	0.371	3.20	12.60	>13.83	0.78	0.5	0.1477
A	5.83	0.380	30.40	---	---	---	---	0.1477
A	5.63	1.70	11.70	6.69	6.73	0.43	6.5	0.1231
A	5.02	6.59	1.0 *	5.08	5.43	0.31	9.0	----
A	5.28	7.05	4.70	4.85	5.40	0.31	9.0	----
B_1	4.75	6.37	5.44	4.88	5.41	0.31	8.5	----
B_1	4.62	18.3	6.25*	---	4.12	0.31	---	----
B_1	5.02	33.2	6.25*	---	4.10	0.31	---	----
B_1	4.80	46.1	4.00*	---	4.22	0.31	---	----
B_2	5.76	5.71	2.75	5.23	5.74	0.32	---	----
B_2	5.80	1.31	26.99	6.80	7.18	0.46	---	----
C	5.05	8.31	5.0 *	3.17	4.58	0.25	---	----
C	5.68	1.94	10.0 *	6.43	6.50	0.33	---	----

* (angle-of-attack)^2 where read for transition location. Not enough data to establish $\overline{\delta^2}$.

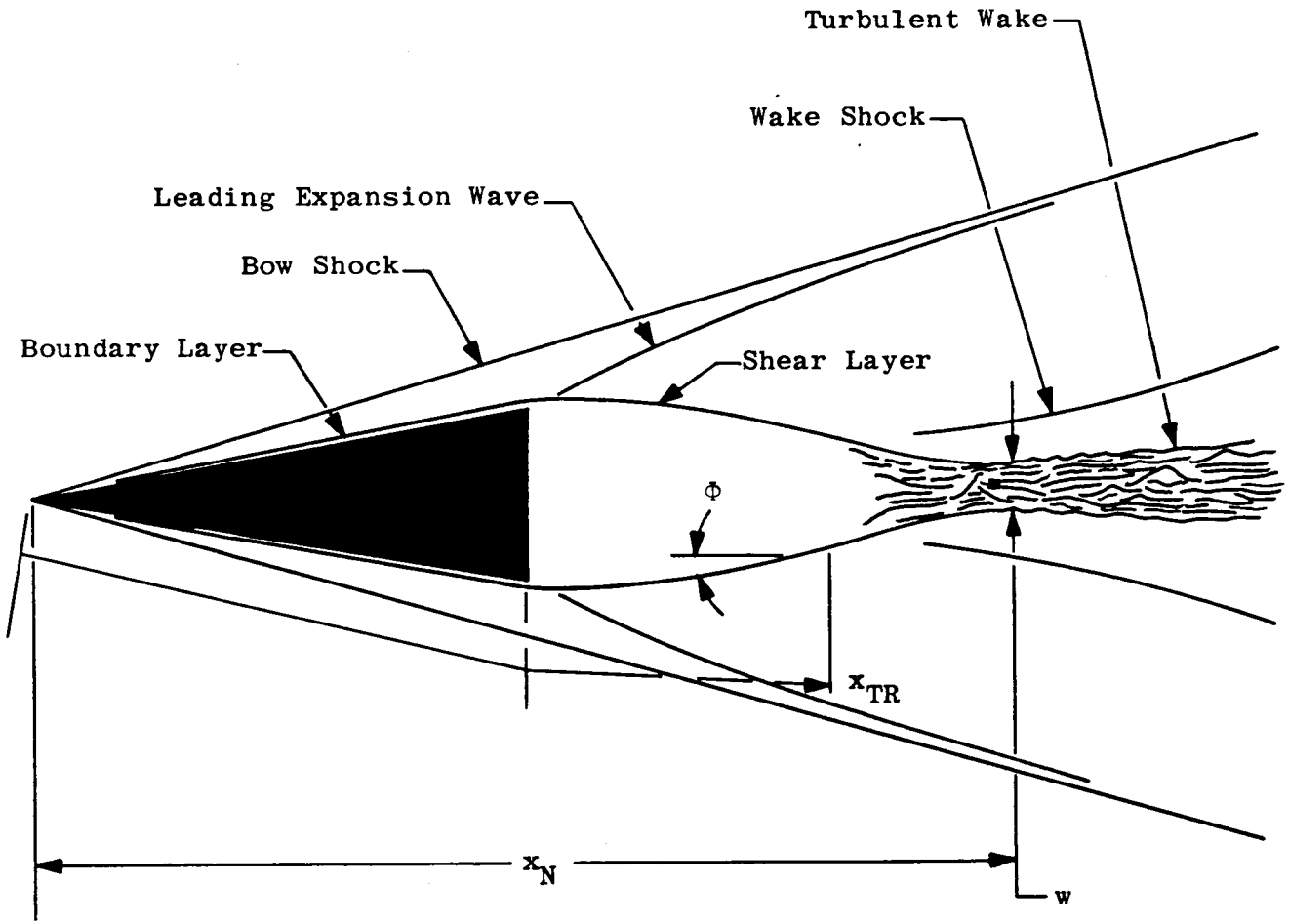


Figure 3. Sketch of the flow field showing some of the tabulated parameters.

body diameters under some conditions.) Accordingly, when one refers to a transition point or transition location, a definition is required. In this report, the point of transition or transition location is that point in the boundary layer, free shear layer, or wake where full turbulence is considered to first exist. Figures 4 through 12 are a series of schlieren and shadowgraph photographs of the models for a range of freestream Reynolds numbers with arrows indicating where the author considers full turbulence to first exist. (It must be noted that the originals show more detail than these reproductions. This is especially true of the color schlieren photographs of low Reynolds number flows.)

Figure 13, page 20, presents transition Reynolds number, based on freestream conditions and length X_{TR}, as a function of freestream body Reynolds number. Because small but finite angles of attack usually existed, and these caused X_{TR} values to differ on opposite sides of the flow fields pictured, it was necessary to distinguish between "windward" and "leeward" flow regions in giving X_{TR} data. Each transition point for the present data represents the arithmetic average of all windward measurements (schlieren and shadowgraph) for that shot. All the data are contained within a band of ±10 per cent of the mean value. Wake transition measurements obtained with a similar model under

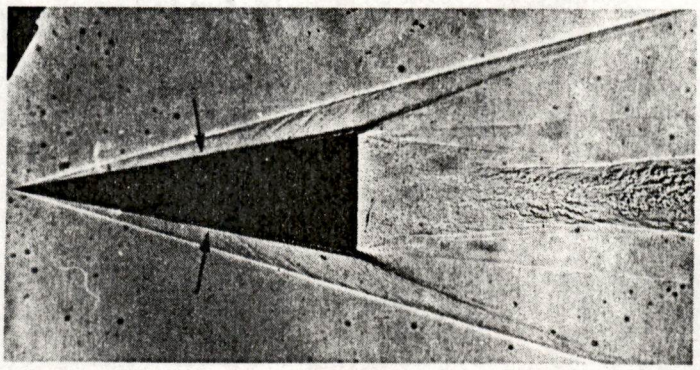


Figure 4. Parallel-light shadowgram of model A, $Re_{\infty,D} = 3.7 \times 10^6$, $M_\infty = 5.1$.

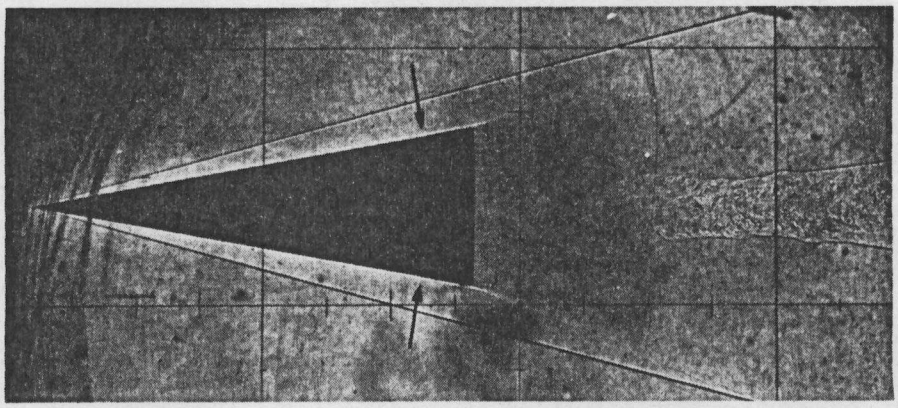
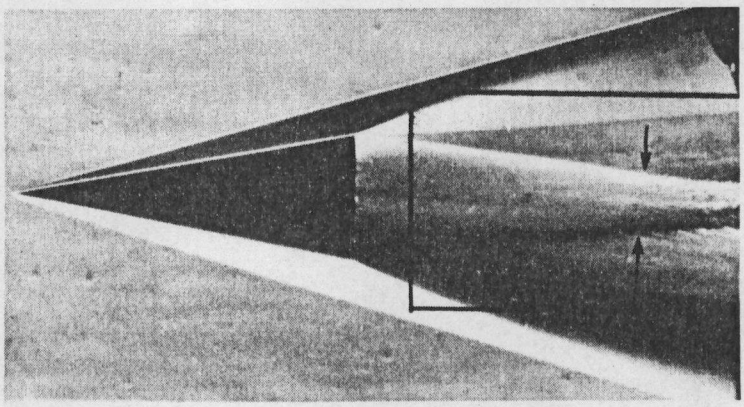
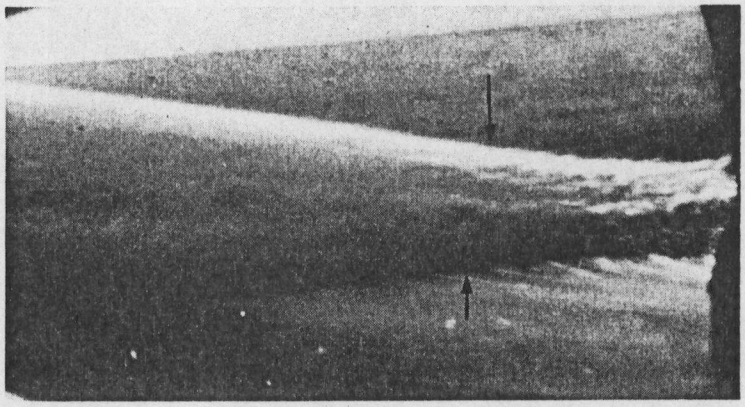


Figure 5. Point-light-source shadowgram of model A, $Re_{\infty,D} = 1.41 \times 10^6$, $M_\infty = 5.3$.

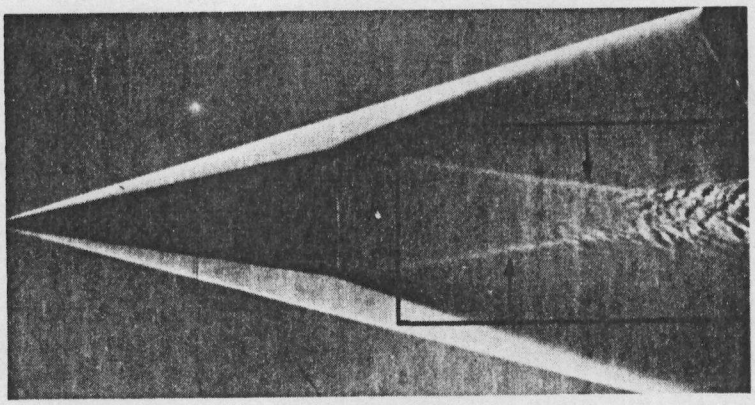


a. Photograph of flow field.

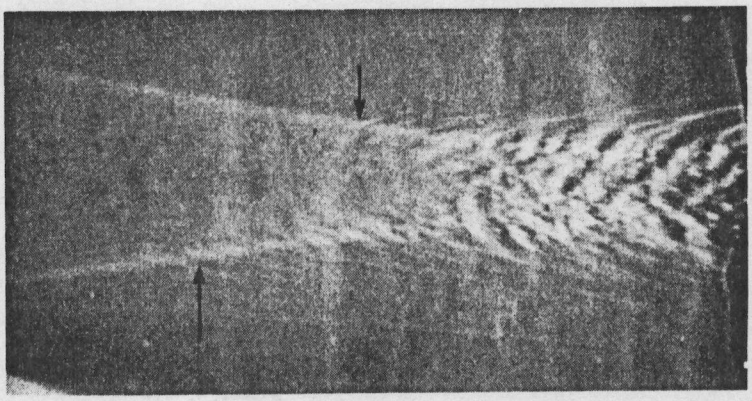


b. Enlargement of free shear layer.

Figure 6. Horizontal knife-edge black-and-white schlieren photograph of model A, $Re_{\infty,D} = 6.59 \times 10^5$, $M_\infty = 5.02$.



a. Photograph of flow field.



b. Enlargement of free shear layer.

Figure 7. Vertical knife-edge black-and-white schlieren photograph of model A, $Re_{\infty,D}$ = 7.05×10^5, $M_\infty = 5.28$.

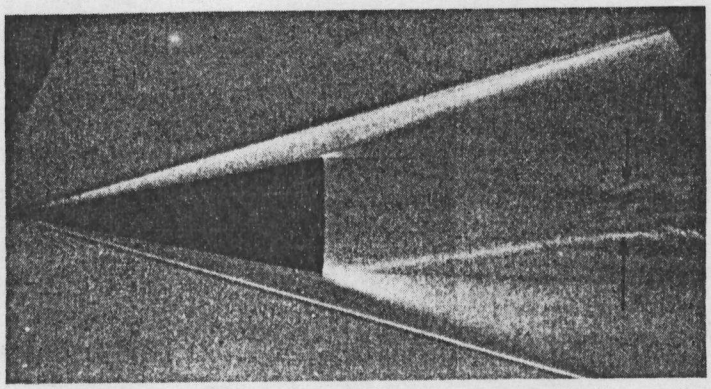


Figure 8. Color schlieren photograph of model A, $Re_{\infty,D} = 3.64 \times 10^5$, $M_\infty = 5.3$.

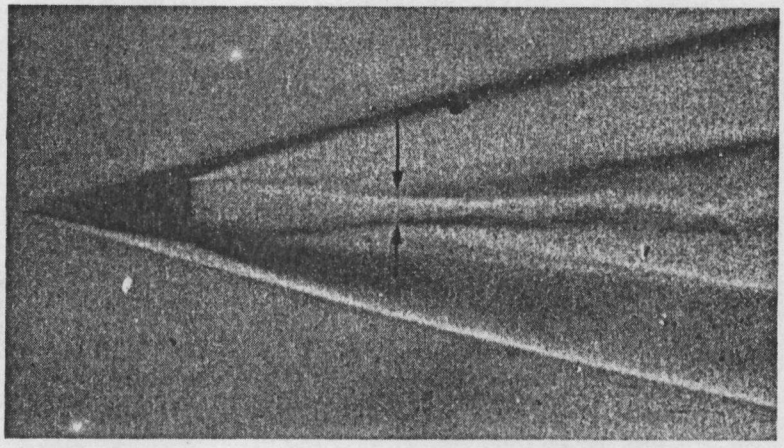


Figure 9. Black-and-white schlieren photograph of model A, $Re_{\infty,D} = 1.7 \times 10^5$, $M_\infty = 5.6$.

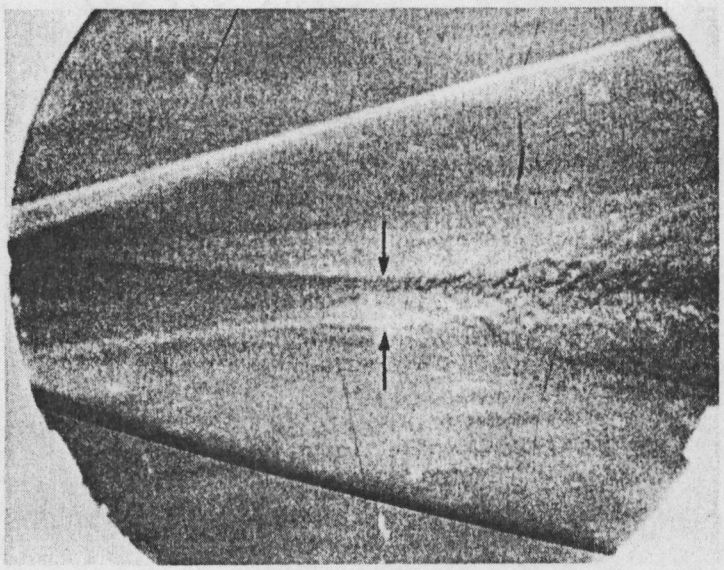


Figure 10. Color schlieren photograph of model A, $Re_{\infty,D} = 1.81 \times 10^5$, $M_\infty = 5.4$.

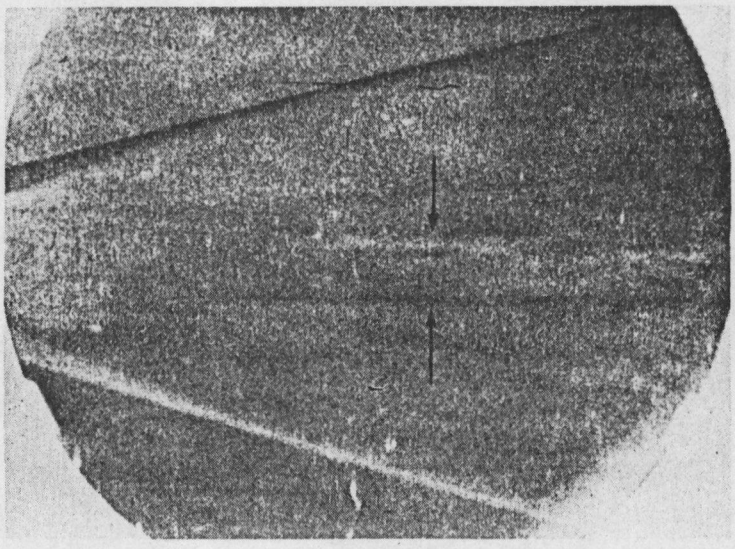


Figure 11. Color schlieren photograph of model A, $Re_{\infty,D} = 7.4 \times 10^4$, $M_\infty = 5.4$.

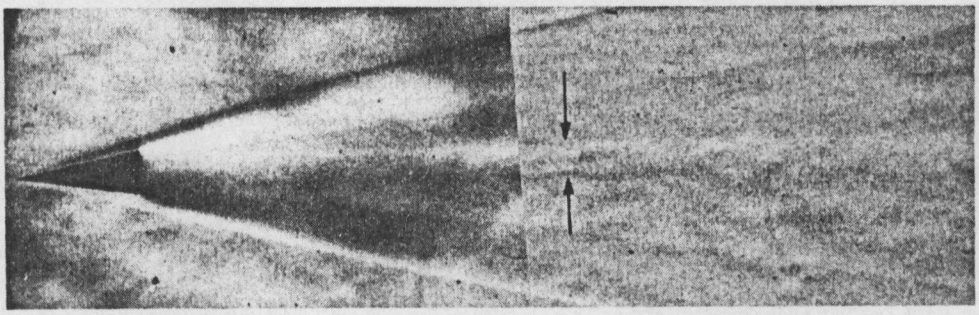


Figure 12. Two frames of black-and-white drum camera schlieren photograph of model A, $Re_{\infty,D} = 3.71 \times 10^4$, $M_\infty = 5.7$.

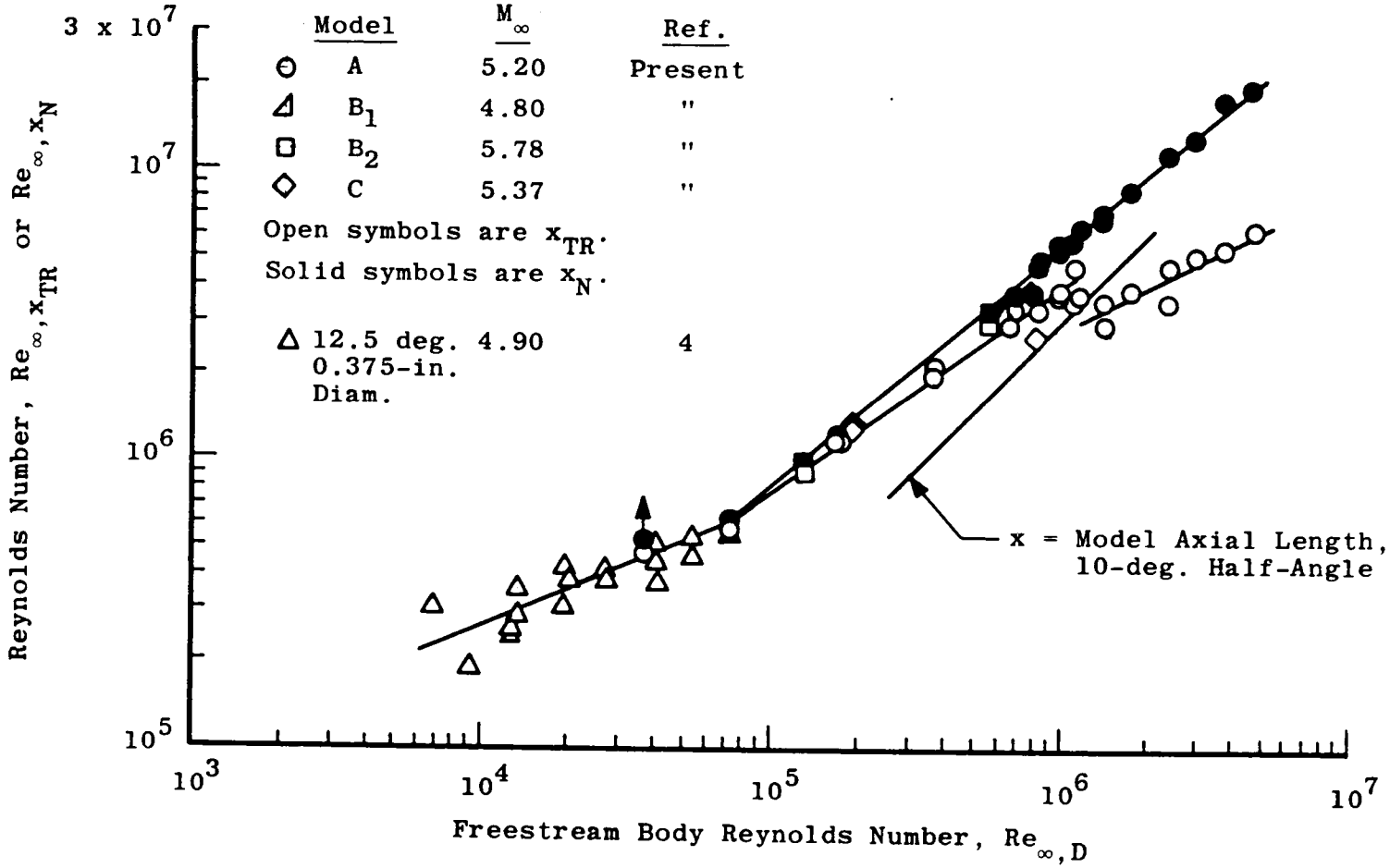
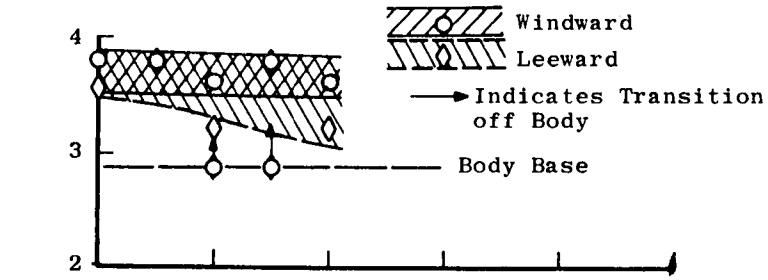


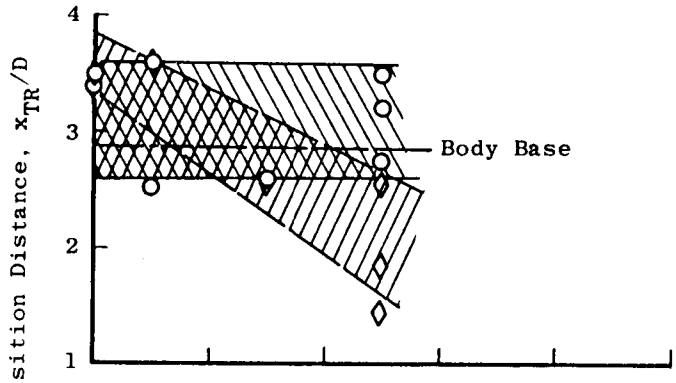
Figure 13. Variation of transition and neck Reynolds numbers with freestream body Reynolds number.

similar flight conditions (4) are compared with the present data. To illustrate the relation of transition location with the neck location, Re_{∞,X_n} is also plotted in Figure 13, page 20.

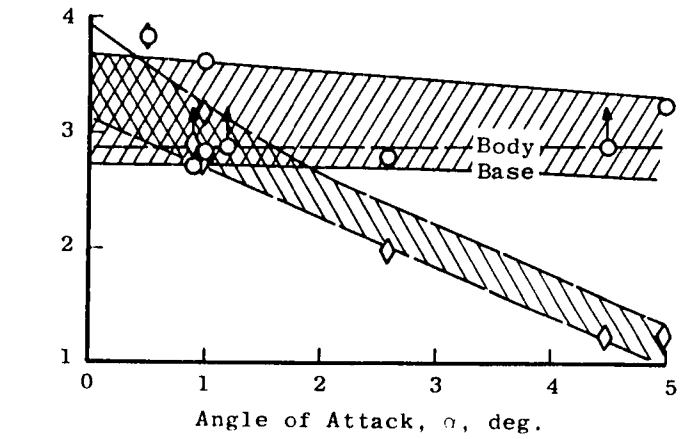
The three data points at a body Reynolds number of 1.1×10^6 in Figure 13 should be discussed separately since the transition location is very near to the body base at this condition. When individual windward and leeward measurements were plotted as a function of model angle of attack, as shown in Figure 14, for each of three flights, a general trend of decreasing distance to transition with increasing angle of attack is seen for the leeward data. This is a result of a cross-flow which will thicken and destabilize the boundary layer on the leeward side. Browand, et al. (5), have indicated that a pair of vortices will be shed from the nose on the leeward side even at very small angles-of-attack (on the order of 8 per cent of the cone half-angle). These would also cause instabilities in the boundary layer which would cause transition to move forward with increasing angle of attack. However, there appears to be little movement with angle of attack for the windward data. Transition on one shot (Figure 14a) was consistently off the body in all photographs for angles as high as 2.5 degrees. Windward data for the other two shots (Figures 14b and 14c) were very inconsistent with angle-of-attack,



a. $Re_{\infty,D} = 1.13 \times 10^6$, $M_\infty = 4.97$.



b. $Re_{\infty,D} = 1.18 \times 10^6$, $M_\infty = 5.26$.



c. $Re_{\infty,D} = 1.12 \times 10^6$, $M_\infty = 5.00$.

Transition Distance, x_{TR}/D

Figure 14. The effect of angle-of-attack on transition distance when transition occurs near to the base for model A.

appearing both on and off the body for angles-of-attack of 0.5 degrees or larger. It can only be concluded that near to the base wake transition is very sensitive to slight variations in the local flow properties.

The discontinuity due to the sudden "jump" of transition as it moves off the body is not unexpected since the supersonic free shear layer has been shown to be relatively stable with respect to flow disturbances (6). This discontinuity as transition leaves the body marks the beginning of the second region, i.e., transition in the separated wake upstream of the wake neck or closure. Transition is close behind the body and moves downstream very slowly as the Reynolds number is decreased. The phenomenon of transition "sticking" in the near wake, as shown to exist behind blunt bodies at high speeds (3) is not demonstrated here, since transition sticking would be characterized by a straight line with a slope of 45 degrees in Figure 13, page 20.

The third region follows where transition moves downstream somewhat faster as the Reynolds number is decreased. While it may be argued that the data could have also been fitted with a smooth curve instead of two straight lines, two slopes do exist in the data and straight lines were drawn to emphasize this point. A possible reason for the two slopes will be discussed later. However, this region should be followed by a fourth region, not shown by the data,

but suggested by Lees (7). In this region transition moves out rapidly to "infinity" and Lees has defined the Reynolds number at which this occurs as the "minimum critical" Reynolds number. For Reynolds numbers less than the "minimum critical" value an instability in the wake would be damped out by the relatively strong viscous forces. For the conditions of this test, Reference (7) suggests that this Reynolds number is $1.0 \times 10^3 < Re_{\infty,D} < 2.0 \times 10^3$.

A study of Figure 13, page 20, shows that no significant region of a constant transition Reynolds number exists within the scope of these data.

Also shown in Figure 13 is the axial position of the wake neck, represented by Re_{∞,X_n}. The neck moves downstream with decreasing freestream Reynolds number. Of some interest is the fact that the neck is just downstream of the location of transition when X_{TR} lies between the body base and the neck. Thus, transition is occurring in a convergent, non-isentropic flow of steep gradients in this second region. The process of formation of the neck is shown in Figures 6 and 7, pages 13 and 14. Figure 6 is a horizontal knife-edge schlieren photograph and Figure 7 is a vertical knife-edge photograph at the same flow conditions. At the lowest body Reynolds number tested (3.71×10^4), the resolution of the schlieren photographs is not sufficient to determine whether

or not a neck existed. This neckless wake is not unique, but has been reported in References (8) and (9). The free shear layer could be seen and appeared to have a constant diameter until turbulence appeared, when it began to increase in diameter. No neck shock could be seen in the flow field at this condition, but the apparent lip shock could be seen extending to at least 35 body diameters from the body base. At this point the shocks were too far apart radially to be seen in the 30 inch diameter schlieren field of view. Figure 13, page 20, shows that the neck and location of transition tend to coincide for $Re_{\infty,D} \approx 10^5$ under present conditions.

From the variation of the neck and transition locations with freestream body Reynolds number, it is suggested that the recompression (and attendant local shocks as shown in Figures 6 and 7, pages 13 and 14) of the free shear layer controls the location of transition until the Reynolds number is low enough so that a neck does not exist. That is, the recompression gradient behind the body would become weak and would not aggravate any instabilities in the flow. For $Re_{\infty,D} < 10^5$ flow instabilities as discussed by Gold (10) would control the location of transition. The Reynolds number where the neck location would no longer control the location of transition would, in turn, be a function of other parameters, such as body shape and Mach number.

CHAPTER III

NEAR WAKE GEOMETRY

During the study of the movement of transition from the body to the near wake region, it became evident that the neck geometry is a strong function of Reynolds number. Data correlated by Waldbusser (11 and 12) have not shown such a strong effect.

In Figure 15, the neck location is shown as a function of freestream body Reynolds number. It is readily seen that as the freestream Reynolds number is decreased, the neck moves downstream from the base. As mentioned before, at $Re_{\infty,D} = 3.71 \times 10^4$, the neck is very nebulous and difficult to define so that the position given in Figure 15 represents what is considered to be the minimum distance that the neck can be from the body nose. The correlation shown in References (11) and (12) is invariant with Reynolds number.

Figure 16, page 28, shows the neck diameter plotted as a function of freestream body Reynolds number. For $Re_{\infty,D} > 10^6$, the neck diameter is constant and has a value of $w/D = 0.3$. For $Re_{\infty,D} < 10^6$, the neck diameter increases with decreasing body Reynolds number and reaches a value of almost $w/D = 0.8$ at the lowest Reynolds number tested. The data of References (11) and (12) are similar to the present

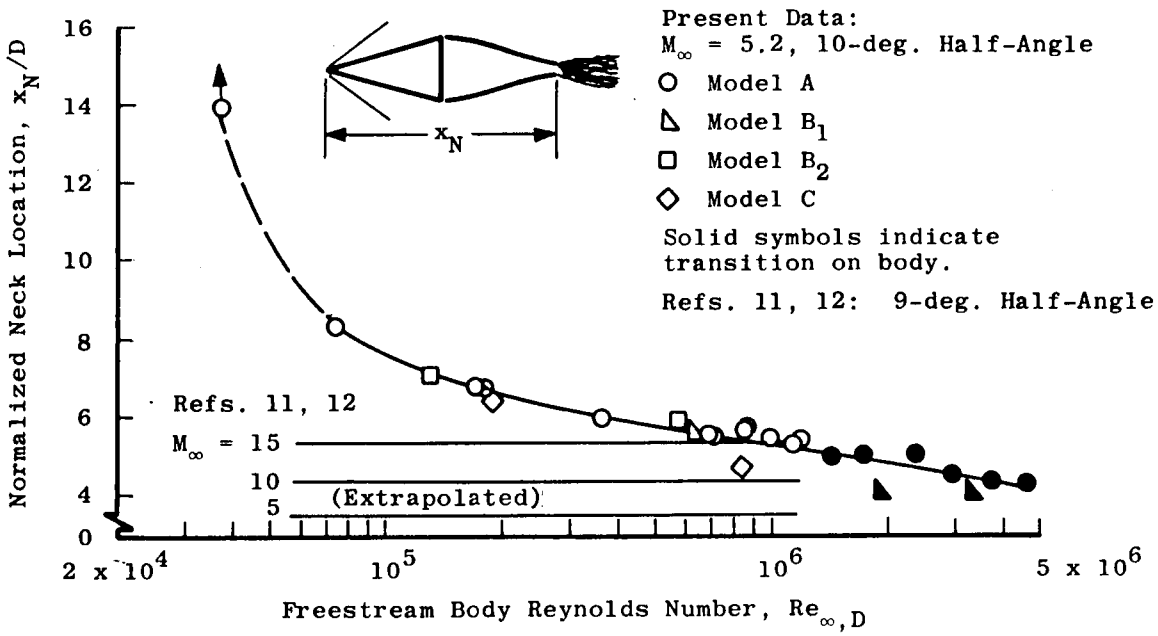


Figure 15. The variation of neck location as a function of freestream body Reynolds number.

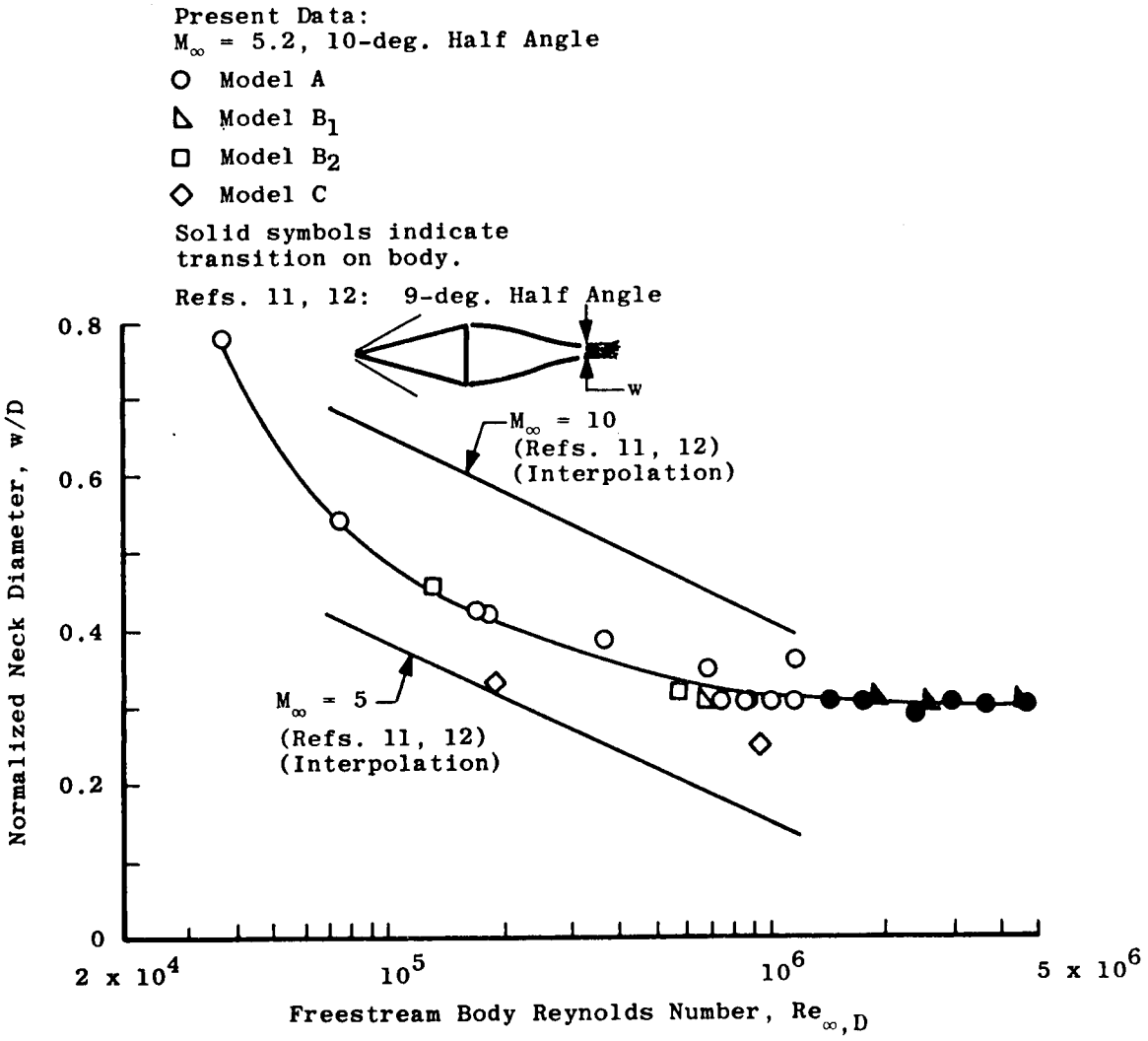


Figure 16. The variation of neck diameter as a function of freestream body Reynolds number.

data in that they predict the same general growth rate, but yield a different diameter.

The wake closure angle is shown as a function of freestream body Reynolds number in Figure 17. This angle was measured at the midpoint of the distance between the body base and the neck. If the free shear layer is assumed to be straight, then the closure angle may be calculated from the measured neck diameter and its location as follows:

$$\Phi = \tan^{-1}\left[\left[(1 - w/D)/2\right] \Big/ \left[X_n/D - 2.83\right]\right] . \qquad (2)$$

A comparison of the measured and calculated values of Φ indicates that the assumption of a straight shear layer will result in a value for Φ that is less than the measured value by about two degrees when $Re_{\infty,D} < 1.2 \times 10^6$, or when transition occurs off the body. For $Re_{\infty,D} > 1.2 \times 10^6$, or when transition occurs on the body, the free shear layer is curving so steeply that it no longer is typified by one particular closure angle and the straight line assumption breaks down. The data of Reference (12) indicate a similar slope, but there is a shift of approximately 9 degrees for equal M_∞. It must be recognized that accurate measurement of this angle is extremely difficult under some conditions, and a degree of individual judgement enters into its determination.

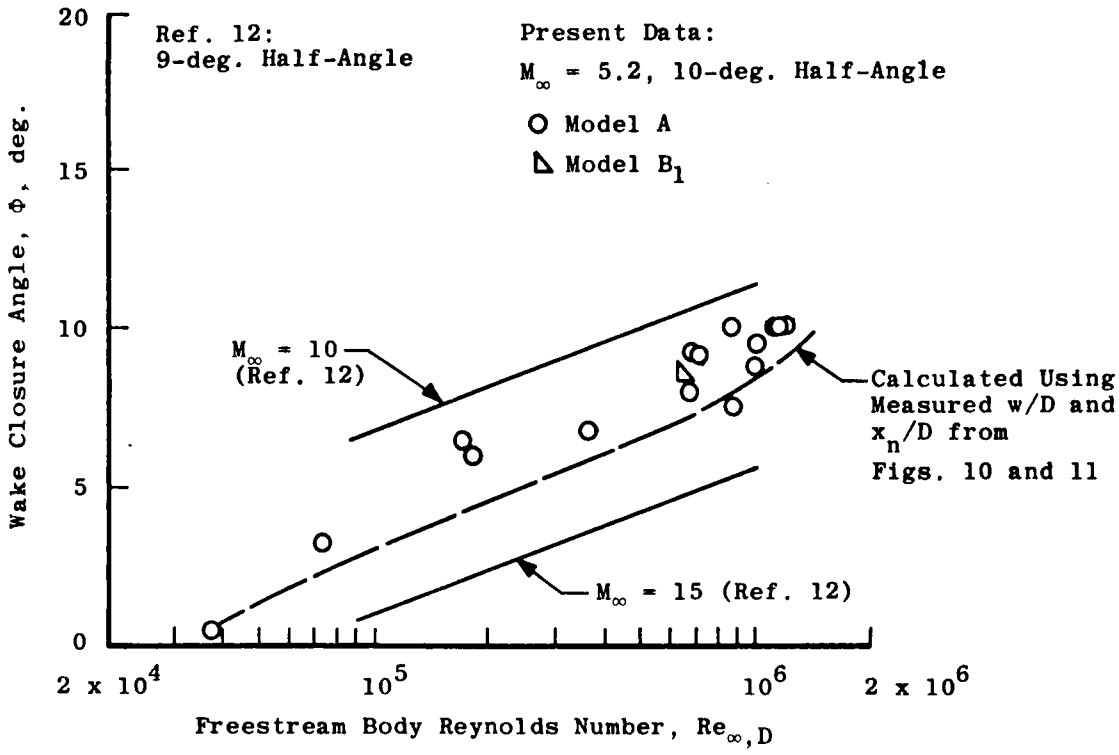


Figure 17. The variation of wake closure angle as a function of freestream body Reynolds number.

In order to show the physical relationship between free shear layer shape, neck location and size, and transition location, some of the photographs were used to construct a map of the base flow region. This is shown in Figure 18 where the edge of the free shear layer and corresponding transition locations are shown in normalized coordinates with freestream body Reynolds number as a parameter. What is believed to be the lip shock also is indicated. This shock shape did not vary with Reynolds number for the range of Reynolds number covered, which is somewhat unexpected. It is interesting to note that what appears to be a second shock also was seen at the corner under some conditions, as shown in the photograph of Figure 4, page 11, and the sketch of Figure 19, page 33. This second shock was observed only for $Re_{\infty,D} > 1.4 \times 10^6$ and did not change shape for the very limited range of Reynolds number over which it was observed. The causes of this shock, if indeed it is a shock, are not known at present and in the absence of detailed wake surveys yielding local flow conditions it is possibly dangerous to speculate on the causes and nature of these apparent shocks. It can be shown that the final wave of the expansion fan originating at the cone base corner would nearly coincide with what is herein called the lip shock in many of these photographs.

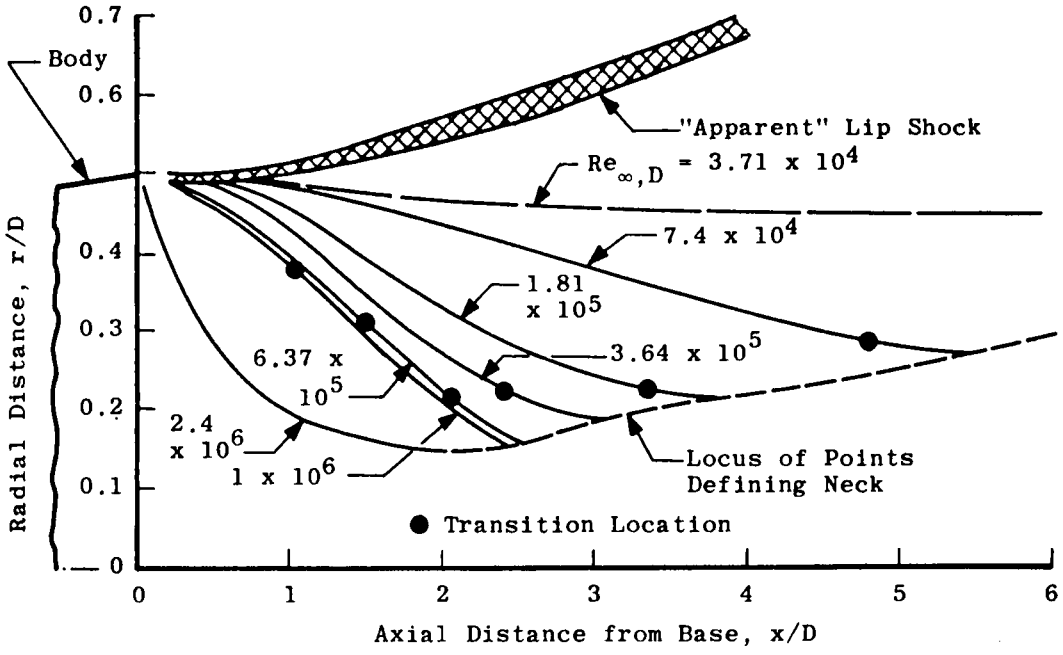


Figure 18. Map of the base flow region.

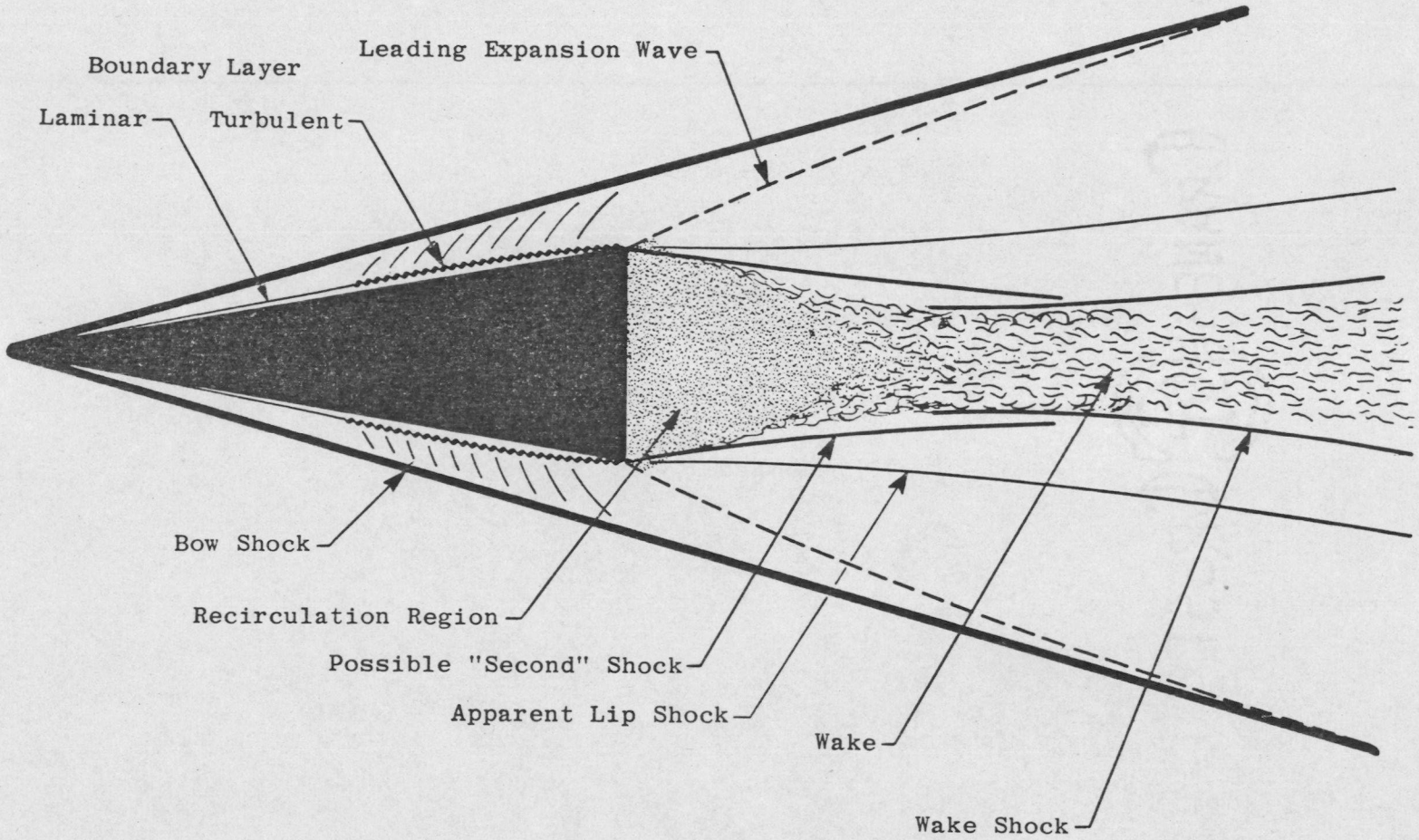


Figure 19. Sketch of the flow field showing the base flow pattern for high Reynolds number.

The near wake survey data of Ragsdale and Darling (13) for a 9-degree half-angle cone suspended in the flow by a system of wires with an adiabatic wall at $M_\infty = 5$ and $Re_{\infty,D} = 3.2 \times 10^6$ show the bow shock, leading expansion wave, end of the expansion, and neck shock. There is no evidence of a lip shock. However, the data were obtained no closer to the base than 0.55 base diameter and the lip shock may have been weakened by the expansion to the point where it could no longer be detected. Further, the schlieren photographs shown were obtained with a vertical knife-edge so that a nearly horizontal weak shock would probably not show up.

Browand, et al. (5) have obtained wake survey data using a magnetic suspension system to support a 7-degree half-angle cone with $M_\infty = 4.3$ and $Re_{\infty,D} = 4.06 \times 10^4$ and an adiabatic wall. A weak lip shock is shown in the pitot profile data, but the Reynolds number is much too low to compare directly with the present data.

Hama (14) has conducted an extensive investigation of the lip shock on a 6-degree half-angle wedge with an adiabatic wall at freestream Mach numbers from 2.01 to 4.45 and wedge surface Reynolds numbers from 3.75×10^5 to 4×10^4, based on base height. The data show that the lip shock orientation is a strong function of both Mach number and Reynolds number for the ranges covered. It was found that

the lip shock had substantial strength and was apparently caused by viscous separation effects.

Bauer (15) has obtained pitot profiles behind a 12-degree half-angle cone at $M_\infty = 3.035$ and $Re_{\infty,D} = 1.13 \times 10^5$ that show a weak lip shock. The model was supported by a cantelevered strut extending upstream from the model nose.

Compared with the present data, the results of these other investigations indicate that (a) what is herein called the lip shock lies at a position consistent with the findings of References (5) and (15), (b) the insensitivity of the lip shock to variations of freestream Reynolds number reported here is at variance with the measurements for wedges reported in Reference (14) and cannot be explained at this time, (c) location of the lip shock at the terminal boundary of the expansion fan noted in the present work is in agreement with Reference (14), but this may not represent a general situation.

CHAPTER IV

DRAG ANALYSIS

Where possible, drag coefficients were obtained to determine whether the turbulent drag rise location agreed with the schlieren observations as to when transition moved off the body. The data were all reduced to zero angle of attack values by using the usual equation:

$$C_{D_o} = C_D + C_{D_\delta} \overline{\delta^2} \quad . \tag{3}$$

The value of C_{D_δ} was established from Reynolds number conditions where more than one data point existed. A slope of 2.5/radian^2 was used for the laminar body conditions and a slope of 3.82/radian^2 for the turbulent body conditions. Since the average value of $\overline{\delta^2}$ was about 4.7 degrees^2, this change amounted to about one-half per cent average correction to the data. The plot of C_{D_o} as a function of freestream length Reynolds number is shown in Figure 20. The Reynolds number where transition leaves the body as observed from schlieren photographs is marked in Figure 20 and agrees well with the drag data prediction.

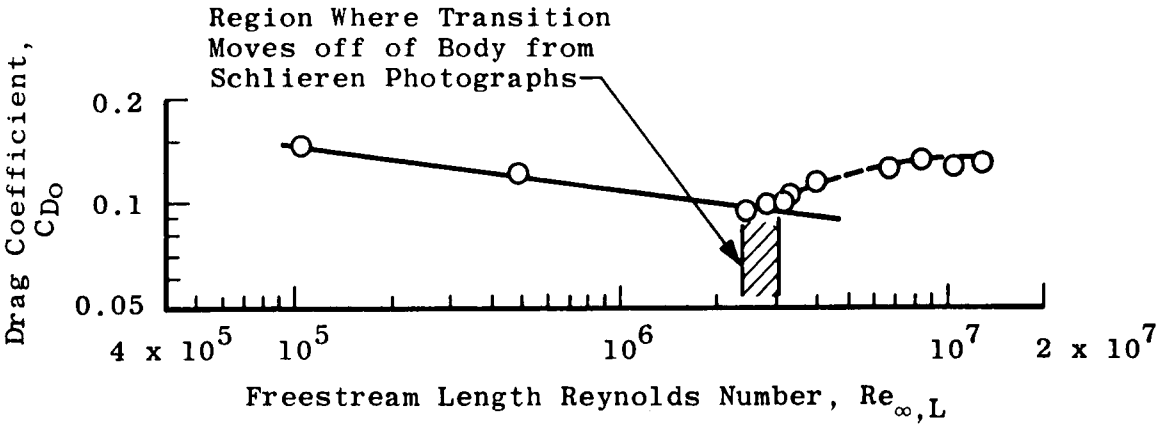


Figure 20. The variation of drag coefficient with freestream length Reynolds number.

CHAPTER V

CONCLUSIONS

For the conditions of this investigation ($M_\infty = 5.2$, $T_w/T_{aw} = 0.18$, and $R_n/R_b = 0$) the following statements may be made:

1. Transition does not jump from the body to the wake downstream of the neck as the Reynolds number is decreased, but will jump into the region upstream of the neck and remain there for a wide range of Reynolds number.
2. The neck geometry is a strong function of Reynolds number. The neck moves downstream and increases in diameter with decreasing Reynolds number. There is a possibility that the neck does not exist for $Re_{\infty,D} < 8 \times 10^5$ under the condition of this test.
3. The neck shock, or recompression shock, weakens with decreasing Reynolds number. The initial lip shock shape does not appear to be a function of Reynolds number for the range of body Reynolds number investigated, provided it is correctly identified in the present case where only photographic observations were made.

4. The Reynolds number of the turbulent drag rise agreed very well with schlieren observations of the location of transition.

These Reynolds number effects on the base flow field will have to be taken into account when designing mathematical models to describe this region. Efforts will have to be made to determine the effects of Mach number and body shape on these variables.

BIBLIOGRAPHY

BIBLIOGRAPHY

1. Cheng, H. K. "Recent Advances in Hypersonic Flow Research," American Institute of Aeronautics and Astronautics, 1:295-310, February, 1963.

2. Lykoudis, P. S. "A Review of Hypersonic Wake Studies," The Rand Corporation RM-4493-ARPA, Santa Monica, California, May, 1965.

3. Wilson, L. N. "Body Shape Effects on Axisymmetric Wakes," General Motors Defense Research Laboratories GM-DRL-TR-64-02k, Santa Barbara, California, October, 1964.

4. Slattery, R. E., and W. G. Clay. "The Turbulent Wake of Hypersonic Bodies," American Rocket Society 17th Annual Meeting and Space Flight Exposition Preprint Number 2673-62, Los Angeles, California, November, 1962.

5. Browand, F. K., M. Finston, and D. K. McLaughlin. "Wake Measurements Behind a Cone Suspended Magnetically in a Mach Number 4.3 Stream," AGARD Conference Proceedings Number 19 (Preprint), Fluid Physics of Hypersonic Wakes, 64 Rue de Varenne, Paris 7e, France, May, 1967.

6. Chapman, D. K., D. M. Kuehn, and H. K. Larson. "Investigation of Separated Flows in Supersonic and Subsonic Streams With Emphasis on the Effect of Transition," National Advisory Committee for Aeronautics Report 1356, Washington, D. C., 1958.

7. Lees, L. "Hypersonic Wakes and Trails," American Institute of Aeronautics and Astronautics, 2:417-428, March, 1964.

8. Au, R. H. C. "An Investigation of the Compressible Laminar Wake Behind a Long Slender Cylinder," University of California, College of Engineering Report AS-66-14, Berkeley, California, September, 1966.

9. Murman, E. M., C. W. Peterson, and S. M. Bogdonoff. "Diagnostic Studies of Laminar Hypersonic Cone Wakes," AGARD Conference Proceedings Number 19 (Preprint), Fluid Physics of Hypersonic Wakes, 64 Rue de Varenne, Paris 7e, France.

10. Gold, H. "Stability of Laminar Wakes," Doctoral dissertation, California Institute of Technology, Pasadena, California, 1963.

11. Waldbusser, E. "Geometry of the Near Wake of Pointed and Blunt Hypersonic Cones," American Institute of Aeronautics and Astronautics, 4:1874-1875, October, 1966.

12. Waldbusser, E. "Geometry of the Near Wake of Pointed and Blunt Hypersonic Cones," General Electric Fluid Mechanics Component Data Memo 1:19, General Electric Company, Valley Forge, Pennsylvania, September, 1964.

13. Ragsdale, W. C. and J. A. Darling. "An Experimental Study of the Turbulent Wake Behind a Cone at Mach 5," U. S. Naval Ordnance Laboratory NOLTR 66-95, White Oak, Maryland, September, 1966.

14. Hama, F. R. "Experimental Investigations of Wedge Base Pressure and Lip Shock," National Aeronautics and Space Administration TR 32-1033, Washington, D. C., December, 1966.

15. Bauer, A. B., "Some Experiments in the Near Wake of Cones," American Institute of Aeronautics and Astronautics, 5:1356-1357, July, 1967.

APPENDIX

APPENDIX

DESCRIPTION OF TEST APPARATUS

I. VKF 100-FOOT HYPERVELOCITY RANGE K

The range consists of a 100-foot long, 6-foot diameter steel tank. A 14-foot long, 6-foot diameter blast tank is connected to the range by a short spool piece. The sabot is stripped in this tank. For the single-stage gun launches of this experiment, the blast tank was extended 20 feet by the addition of a 14-inch diameter pipe to allow a greater sabot separation time.

Range pressure was monitored with two Hass mercury manometers and one MKS Baratron unit. Measurement errors using this system, over the range of pressures for this test, was less than 0.062 per cent of reading.

Range temperature was monitored at six stations with copper-constantan thermocouples. System error was $\pm 1.0^{\circ}F$.

Six dual-axis spark shadowgraphs are situated at nominal 15-foot intervals along the range. Optical axes at each station are mutually orthogonal with the range centerline. The centerline field of view of these systems is 12 inches. The spark light sources have an exposure duration of 0.1 microsecond. Time durations which separated the

shadowgraph exposures were measured by 10-megacycle chronographs. Timing resolution was ±0.1 microsecond. Flow field information was obtained from this system for freestream body Reynolds numbers greater than 7.0×10^5.

A high-sensitivity, single-pass schlieren system is positioned 15 feet from the range entrance. The schlieren has a 12-inch diameter field of view. It was used as either a parallel-light shadowgraph, black-and-white schlieren, or a color schlieren system, depending on the sensitivity desired. The color system uses a light source with a duration of 0.2 microsecond. The light source for the black-and-white systems has a duration of 0.1 microsecond.

II. VKF 1000-FOOT HYPERVELOCITY RANGE G

The range consists of a 1000-foot long, 10-foot diameter steel tank. A blast chamber, which absorbs the muzzle gases and provides a sabot trap, makes up the initial 85 feet of the range.

Pressures were monitored at three stations along the range using MKS Baratron units. Measurement errors using this system did not exceed 1 per cent of reading.

Range temperatures were monitored at three stations using copper-constantan thermocouples. System error was $\pm 1.0^{\circ}F$.

Forty-three dual-axis, spark shadowgraphs are located at nominal 20-foot intervals along the range. Optical axes at each station are mutually orthogonal with the range centerline. The centerline field of view of these systems is 30 inches. The spark light sources have an exposure duration of 0.12 microsecond. Timing resolution between the stations is $\pm$0.1 microsecond.

A high-sensitivity, single-pass schlieren system is positioned 156 feet from the range entrance. The schlieren has a 30-inch diameter field of view and is operable in either single-frame or multi-frame modes. In the latter, as many as 20 frames are obtained. Exposure duration is 0.1 microsecond.